Journal of Photochemistry and Photobiology A: Chemistry 222 (2011) 210–219

Contents lists available at ScienceDirect

Journal of Photochemistry and Photobiology A: Chemistry

journal homepage: www.elsevier.com/locate/jphotochem

# The nascent OH detection in photodissociation of 2-(bromomethyl)hexafluoro-2-propanol at 193 nm: Laser-induced fluorescence study

Yogesh N. Indulkar[a,b], Hari P. Upadhyaya[a], Awadhesh Kumar[a], Suresh B. Waghmode[b], Prakash D. Naik[a,*]

[a] Radiation & Photochemistry Division, Bhabha Atomic Research Centre, Trombay, Mumbai-400 085, India
[b] Department of Chemistry, University of Pune, Ganeshkhind, Pune-411 007, India

ARTICLE INFO

*Article history:*
Received 24 September 2010
Received in revised form
20 December 2010
Accepted 24 January 2011
Available online 12 June 2011

*Keywords:*
Fire extinguisher
Laser photolysis
Dynamics
Halogenated alcohol
OH formation
Energy partitioning

ABSTRACT

Photodissociation of 2-(bromomethyl)hexafluoro-2-propanol (BMHFP) and 3-bromo-1-propanol (BP), involving $\sigma^*_{C-Br} \leftarrow n_{Br}$ transition at 193 nm, has been investigated by measuring laser-induced fluorescence spectra of the expected OH product. The OH channel is a minor dissociation pathway with a quantum yield of $0.17 \pm 0.05$ in BMHFP, whereas it was not observed in BP. Partitioning of the available energy into translation, rotation, and vibration of the photoproducts has been measured by state selective detection of the nascent OH product in BMHFP. OH is produced mostly in the ground vibrational level ($v'' = 0$), with a rotational distribution being characterized by a temperature of $465 \pm 25$ K. But, a significant fraction of the available energy of 30.2 kcal mol$^{-1}$ is partitioned into translation of OH (14.6 kcal mol$^{-1}$). The OH($v'' = 0, J''$) populations in the spin-orbit states as well as in the $\Lambda$-doublet states are statistical. A plausible mechanism of OH formation on excitation of BMHFP at 193 nm is suggested, with the primary reaction channel being elimination of Br atom by direct C–Br bond dissociation from a repulsive surface. The Br radical is detected using (2 + 1) resonance-enhanced multiphoton ionization (REMPI) at ~234 nm. It is produced in both the ground ($^2P_{3/2}$) and the excited ($^2P_{1/2}$) spin-orbit states with the relative quantum yield of the latter to be 0.36. The co-fragment of Br undergoes secondary C–O bond dissociation to produce OH and $F_3C–C(=CH_2)–CF_3$, with the reaction having a barrier located in the exit channel. In this two-step three-body dissociation process, a major fraction of the available energy is released into translation ($\langle f_T \rangle \sim 0.75$), resulting from an impulsive C–Br bond dissociation in the primary step and presence of an exit barrier in the secondary process. Experimental results combined with theoretical calculations provide a clear picture of the dynamics of OH formation from BMHFP at 193 nm. In addition, the energetics of another channel, competing with OH, have been calculated from the primary product $F_3C–C(CH_2)(OH)–CF_3$. In contrast to BMHFP, the OH product could not be observed from the photolysis of 3-bromo-1-propanol (another saturated halogenated propanol) at 193 nm under the detection limit of the present experimental condition, although it has a higher absorption cross-section at 193 nm.



## 1. Introduction

Photodissociation dynamics of fluoroalcohols has attracted considerable attention in the past two decades, following the suggestion that fluoroalcohols can be potential fire extinguishing agents as an alternative to Halon 1301. 3-Bromo-1,1,1-trifluoro-2-propanol (BTFP) is a suggested fire extinguisher with its cup burner value of 4.1 and the extinguishing concentration against hydrogen and hydrocarbon flame of 5.7 and 4.0, respectively [1]. Like BTFP, its derivative 2-(bromomethyl)hexafluoro-2-propanol (BMHFP) with the H atom on C (attached to OH) replaced with a $CF_3$ group, can be a potential fire extinguishing agent. However, no reports on photochemistry and kinetics of BMHFP are available in the literature. The removal pathways of these compounds from the atmosphere are not known. Several processes, such as reaction with OH, photolysis, wet deposition and dry deposition, can remove these compounds. Solar photolysis should not contribute significantly in the troposphere, but expected to be a viable loss mechanism in the stratosphere, because of the availability

* Corresponding author. Tel.: +91 2225595398; fax: +91 2225505151.
*E-mail addresses:* yogesh_unichem@yahoo.co.in (Y.N. Indulkar), haripu@barc.gov.in (H.P. Upadhyaya), awadesh@barc.gov.in (A. Kumar), suresh@chem.unipune.ernet.in (S.B. Waghmode), pdnaik@barc.gov.in, pd1959@rediffmail.com (P.D. Naik).

1010-6030/$ – see front matter © 2011 Elsevier B.V. All rights reserved.
doi:10.1016/j.jphotochem.2011.01.026

of shorter wavelengths in the solar spectrum. To understand the photolytic behavior of BTFP, in our previous work we investigated its photodissociation dynamics at 193 nm in the gas phase [2], and detected the OH radical as a transient product among other products. Combined with experimental and theoretical studies, a plausible mechanism for this reaction channel was reported. Similar to BTFP, BMHFP photodissociation is also expected to be a potential source of bromine atom and hydroxyl in the atmosphere. To investigate the nature of photodissociation dynamics of BMHFP, a study on its photodissociation is necessary.

In photodissociation of saturated alcohols, such as methanol [3], ethanol [4], 1-propanol and 2-propanol [5], after the $\sigma^*_{(O-H)} \leftarrow n_{(O)}$ excitation, the O–H bond breaking is the predominant pathway, and this fast dissociation process occurs on the repulsive excited state potential energy surface (PES) along the O–H coordinate with a large translational energy release. In general, in all these saturated alcohols the C–OH bond cleavage leading to OH formation is a minor channel, and many times not observed, even with a sensitive laser-induced fluorescence (LIF) technique, on excitation of these alcohols at 193 nm. The OH channel is not observed mainly because of presence of a barrier resulting from an avoided curve crossing in this dissociation channel. In contrast, photo-excitation of unsaturated alcohols, such as propargyl [6] and allyl [6,7] alcohols at 193 nm, which involves $\pi^* \leftarrow \pi$ electronic transition, leads to the formation of OH, as detected by LIF. In addition to introduction of unsaturation centre, other structural modifications in saturated alcohols, such as halogenations, can alter the nature of the electronic excitation at 193 nm, and this can facilitate operation of the OH channel from saturated alcohol involving a different reaction mechanism. The photodissociation of halogenated saturated alcohols, 2-bromoethanol and 2-chloroethanol, at 193 nm has been studied experimentally [8], and only one primary channel, halogen atom formation after C–X (X = Br, Cl) bond scission, has been observed. In case of 2-bromoethanol, the co-product $C_2H_4OH$ was reported to undergo secondary dissociation to produce $C_2H_4$ and OH. BTFP [2] is a saturated halogenated alcohol and undergoes photodissociation on excitation at 193 nm, involving $\sigma^*_{(C-Br)} \leftarrow n_{(Br)}$ transition, to produce OH as a secondary product from the primary product $F_3C–CH(OH)–CH_2$, formed by direct C–Br bond scission from a repulsive surface. Thus, photodissociation of these halogenated saturated alcohols at 193 nm involves $\sigma^* \leftarrow n$ transition, and generates OH in the secondary reaction channel. A question arises; do all the halogenated alcohols generate OH on excitation at 193 nm? To address this question, we have investigated photodissociation dynamics of BMHFP, and another brominated saturated alcohol, 3-bromo-1-propanol (BP).

In the present study, we have investigated the photodissociation dynamics of BMHFP and BP at 193 nm under collision-free conditions, and detected the nascent OH photoproduct only from BMHFP, by employing the LIF technique. We have also carried out *ab initio* theoretical calculations to investigate a probable channel that leads to formation of OH and to characterize the nature of the transition state. Partitioning of the available energy among translational, rotational, and vibrational degrees of freedom of the photoproduct, the Λ-doublet distribution, and the spin-orbit population ratio of the OH fragments have been measured. We have also characterized some of the stable photoproducts of BMHFP, employing FTIR absorption spectroscopy, and proposed mechanisms of their formation with the help of both experimental results and molecular orbital (MO) calculations.

## 2. Experimental

To study the photodissociation dynamics of BMHFP, laser photolysis-laser induced fluorescence (LP-LIF) technique was used, which is described in detail in a previous paper [9]. Briefly, the glass reactor had crossed arms at right angles with windows, allowing the photolysis and the probe laser beams to intersect at the centre of the chamber. The photolysis laser used is an excimer laser (Lambda Physik, Model Complex-102, Fluorine version) and the probe laser is a Quantel dye laser with frequency doubling and mixing modules (TDL90) pumped by a seeded neodymium doped yttrium aluminium garnet (Nd:YAG) laser (Quantel model YAG980 E-20). The detector is attached to the bottom window of the glass reactor to view the intersection volume of the photolysis and probe lasers. It consists of a lens of focal length 50 mm (diameter = 38 mm), to collect the fluorescence, photomultiplier tube (Hamamatsu, model R-928P) to detect it, and a band pass filter ($\lambda_{centre}$ = 310 nm, FWHM = 10 nm, $\%T_{310\,nm}$ = 10) placed between the lens and the PMT to cut off the scattering from the photolysis laser. Both laser beams were unfocused and attenuated to prevent any saturation effect or multiphoton event. The photomultiplier output was fed into a boxcar for gate integration and digitization. The scanning of the dye laser, and data acquisition were controlled by a Pentium II personal computer.

The OH fragment was probed state selectively by exciting the $A^2\Sigma \leftarrow X^2\Pi$ (0,0) transition of OH (306–309 nm) and monitoring the subsequent $A \rightarrow X$ fluorescence. A digital delay generator was used to vary the time delay between the photolysis and the probe beams, and all the LIF excitation spectra were measured at the time delay of ~50 ns. The compound in the form of vapor was flowed through the glass reactor with the static pressure ~50 mTorr at a flow velocity of ~10 cm/s, and it was photolyzed by ArF laser at 193 nm. The sample pressure in the cell was measured with a capacitance manometer. The intensities of the photolysis and the probe lasers were separately measured using photodiodes, and measured fluorescence excitation spectra were normalized with the measured lasers intensities. The LIF intensity was found to be linearly proportional to both the photolysis and probe laser intensities.

Absorption cross-section of BMHFP at 193 nm was measured by filling a known pressure of the sample into a 51 cm long cylindrical absorption cell, fitted with $MgF_2$ windows for passing the excimer laser beam. A beam splitter was used for dividing the original laser beam into two parts, one for passing through the sample and the other as a reference. Two photodiodes were used for measuring the intensities of the sample beam, after exit from the sample cell, and the reference beam. By measuring ratio of the intensities of the two beams, the fraction of the intensity absorbed by the sample was determined. This fraction was plotted against the number of molecules in the cell in a semilog plot.

Br is expected to be a photoproduct on UV photodissociation of BMHFP, and an experimental arrangement was made to detect this product. The photodissociation dynamics experiments were performed in a molecular beam condition by combining resonance enhanced multiphoton ionization (REMPI) and time of flight (TOF) mass spectrometer to state-selectively monitor the photoproducts Br ($4P\,^2P_{3/2}$) and Br ($4P\,^2P_{1/2}$) atoms, which are referred to as Br and Br*, respectively. Experimental details are similar to that employed in our earlier work [10]. The (2 + 1) REMPI transitions of Br and Br* atoms, in the wavelength region of 230–235 nm, were used to probe Br and Br* atoms. The laser pulses were generated from a Quantel dye laser, TDL 90, using rhodamine 101 (LC 6400) dye solution in methanol, pumped by a Quantel seeded Nd:YAG laser, YG-981-C-20. The fundamental dye laser output was frequency-doubled in a KDP crystal, and mixed with the fundamental output of the Nd:YAG laser, to obtain an output in the range 230–235 nm. The above laser output was separated from the rest of laser beams, using a set of four Pellin-Broca prisms. In all the REMPI experiments, the same laser beam was employed as a pump and a probe, i.e., for both photodissociation of the parent molecule and ionization of the photoproducts Br and Br* atoms. The laser beam was focused by a

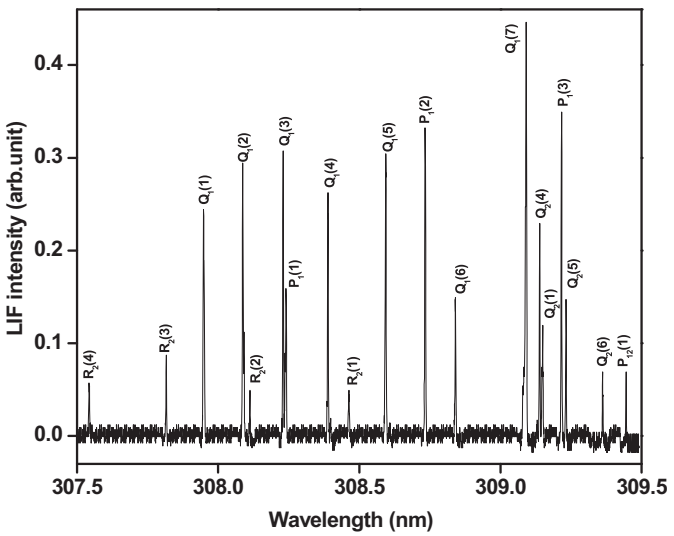


**Fig. 1.** LIF excitation spectrum of the (0,0) band of the $A^2\Sigma^+ \leftarrow X^2\Pi$ system of the nascent OH radical formed in photodissociation of BMHFP (50 mTorr) at 193 nm.

lens of 280 mm focal length. The relative quantum yields of Br and Br* were extracted from the relative integrated signal intensities in the TOF spectrum at 233.70 nm and 234.04 nm, respectively, corresponding to two photon transitions, 6p $^4P_{3/2} \leftarrow 4p\ ^2P_{3/2}$ and 6p $^2S_{1/2} \leftarrow 4p\ ^2P_{1/2}$.

Fourier transform infra-red (FTIR) spectrophotometer (Bruker, model IFS 66v/S) and a glass cell fitted with a pair of ZnSe windows, filled with a known amount of BMHFP (~5 Torr pressure), were used to measure the absorption spectra. To identify the stable photoproducts, FTIR absorption spectra were measured after irradiation at 193 nm for 500 pulses (energy fluence = 40 mJ cm$^{-2}$).

2-(Bromomethyl)hexafluoro-2-propanol (97%, SynQuest Laboratories, Inc.) and 3-bromo-1-propanol (97%, Aldrich) were used after several freeze-pump-thaw cycles in this work.

## 3. Theoretical methods

For a better understanding of the dynamics and the energetics of the experimentally observed photodissociation channels of BMHFP, *ab initio* molecular orbital (MO) calculations were performed, using Gaussian 03 program [11]. The structures of molecular species along with transition states were optimized employing density functional theory (DFT) at the B3LYP level, using 6-311+G(d,p) basis sets. Besides the B3LYP energy, the energies of the optimized structures were calculated also at the second-order Moller–Plesset (MP2) level of theory, using the same basis sets. The harmonic vibrational frequencies and force constants were calculated to ensure that the stationary points on the potential energy surfaces are true local minima. All transition state structures were characterized by only one imaginary frequency and one negative eigenvalue of the force constant matrix.

We also carried out the excited electronic state calculations at the configuration interaction with the single electronic excitation (CIS) level to understand the nature of electronic excitation of BMHFP at 193 nm.

## 4. Results and analysis

### 4.1. Detection of OH

Photolysis of BMHFP at 193 nm produces the OH radical, which was detected employing the LP-LIF technique. However, under similar experimental conditions, OH could not be detected from BP. We probed the quantum state distribution of the nascent OH radical by measuring the fluorescence generated from its A–X system after exciting the same system by a tunable dye laser. The measured LIF signal was found to be linearly dependent on the photolysis and probe laser intensities, indicating that the photodissociation of BMHFP was a single photon process and that the OH molecular transition was not saturated. Rotationally resolved lines could be measured for the (0,0) vibronic band of OH. However, no LIF signal could be measured for the (1,1) band, indicating that the OH radical is generated mostly in the ground vibrational level i.e., $v'' = 0$. The excitation spectra of OH, with several rotational lines for the (0,0) transition, were measured. A typical LIF excitation spectrum of OH, at 50 mTorr pressure and 50 ns time delay between the photolysis and probe lasers, is shown in Fig. 1. We extracted the information on the dynamics of OH formation from the profiles of these rotational lines of the excitation spectrum.

#### 4.1.1. Average rotational energy of OH

The rotational lines of the (0,0) band of the $A^2\Sigma^+$–$X^2\Pi$ system of the OH radical were assigned based on its reported spectral data [12]. Using integrated areas of these measured lines, after normalization with respect to the photolysis and probe laser intensities, pressure of the sample in the cell, and Einstein's absorption coefficients $B_{ij}$ (taken from Ref. [13]), the relative population of each

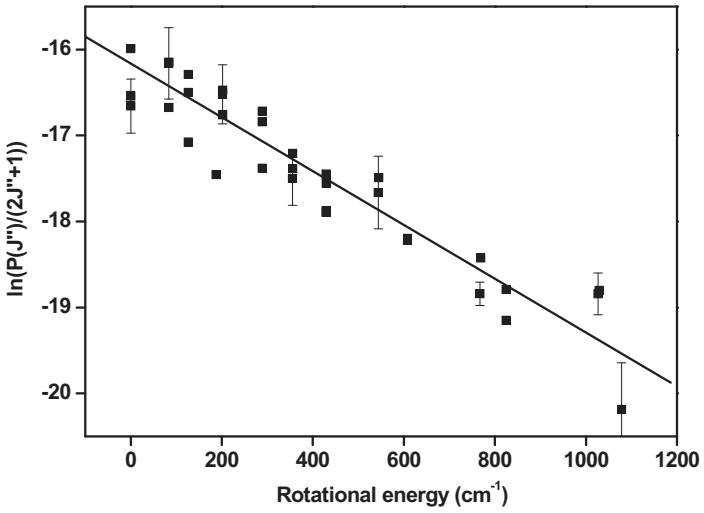


**Fig. 2.** A Boltzmann plot of rotational state population against energy of rotational states of OH ($v'' = 0$) generated in dissociation of BMHFP at 193 nm laser excitation.

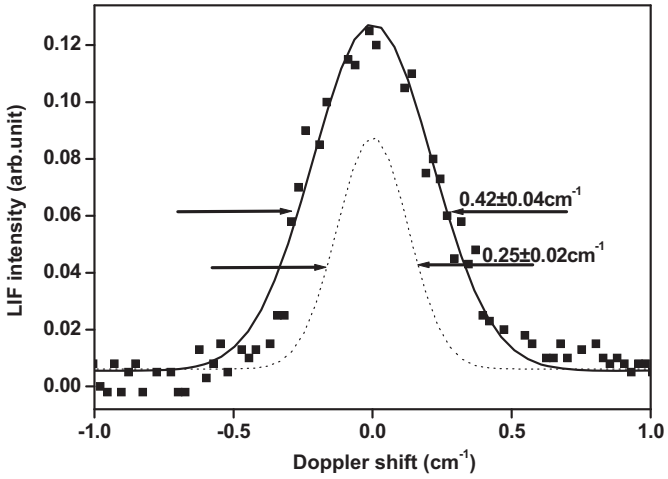


**Fig. 3.** Doppler profile of $P_1(2)$ line of the $A^2\Sigma^+ \leftarrow X^2\Pi\,(0,0)$ system of the OH radical produced in dissociation of BMHFP with 193 nm laser. The dotted line represents the laser spectral profile.

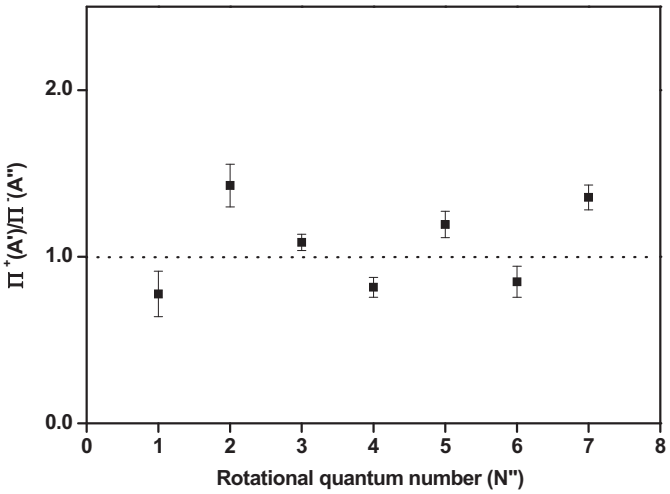


**Fig. 4.** A plot of Λ-doublet population ratio against rotational quantum number $N''$ for the nascent OH formed in laser-induced photodissociation of BMHFP at 193 nm. The plot indicates no preference for any particular Λ-doublet state.

rotational level was calculated. A Boltzmann plot, Fig. 2, was constructed by plotting the corrected populations $P(J'')$ of the nascent OH fragment against energy of the rotational levels ($\varepsilon$), using the equation,

$$\ln\frac{P(J'')}{(2J''+1)} = \frac{-\varepsilon hc}{kT_R} + \text{constant}. \quad (1)$$

The rotational temperature ($T_R$) corresponding to the rotational population distribution of OH($v''=0$), produced on photoexcitation of BMHFP at 193 nm, was calculated from the slope of the plot, to be $465 \pm 25$ K, which implies $0.93 \pm 0.05$ kcal mol$^{-1}$ of the average rotational energy into the OH fragment.

*4.1.2. Average translational energy release in OH*

The average translational energy release in the photoproduct OH can be evaluated using widths of Doppler broadened rotational lines, since the Doppler broadening of the LIF lines is due to molecular velocity of the fragments. A typical Doppler profile of the $Q_1(6)$ line of OH from BMHFP is depicted, after de-convolution, in Fig. 3. Doppler profiles of ten each of $P_1(2)$ and $Q_1(6)$ lines were measured, and after de-convoluting these observed profiles with the instrumental functions, the average Doppler width of $0.42 \pm 0.04$ cm$^{-1}$ is obtained. The Doppler width $\Delta\nu_D$ is related to the temperature ($T_T$) by the equation [14],

$$\Delta\nu_D = 7.16 \times 10^{-7}\nu_0\sqrt{\frac{T_T(OH)}{m_{OH}}}, \quad (2)$$

where $\nu_0$ and $m_{OH}$ are the centre frequency of the rotational line and the mass of OH, respectively. The measured average Doppler width corresponds to the average translational energy in OH, $E_T$(OH) of $14.6 \pm 2.8$ kcal mol$^{-1}$.

*4.1.3. Λ-doublets and spin-orbit states distributions*

An interaction between the rotation of the nuclei and the electronic orbital angular momentum is found to produce a splitting into two components for each $J$ value in the state with $\Lambda \neq 0$, which are otherwise doubly degenerate without rotation [15]. The Λ doublets in a $^2\Pi$ state differ in the relative orientation of the π molecular orbital and the angular momentum $J$. In the classical (high $J$) limit, $^2\Pi^+(A')$ and $^2\Pi^-(A'')$ refer to the π lobes being respectively parallel and perpendicular to the rotational plane. The population in the $\Pi^+$ state is probed by the P or R rotational lines, and that in the $\Pi^-$ state by the Q lines of the excitation spectrum. The ratio of the corrected intensities of P to Q lines was plotted against the corresponding rotational quantum number ($N''$), shown in Fig. 4, and these values are close to unity. The observed statistical distribution in the Λ-doublet states indicates that the OH product has no preference for any particular Λ-doublet state.

The ground electronic state of OH is $^2\Pi$, which splits into two states $^2\Pi_{3/2}$ and $^2\Pi_{1/2}$ due to spin-orbit coupling. The population of the $\Pi_{3/2}$ level of the OH radical is measured by $P_1(N'')$ or $Q_1(N'')$ or $R_1(N'')$ lines, and that of the $\Pi_{1/2}$ level by the intensity of $P_2(N'')$ or $Q_2(N'')$ or $R_2(N'')$ lines. A plot of the ratios of corrected intensities of $P_1(N'')$ and $P_2(N'')$ against $N''$ shows these values to be almost unity and invariant up to $N''=7$ (Fig. 5), implying that the levels are equally populated for all probed rotational levels, and the X $^2\Pi$ spin-orbit components ($^2\Pi_{3/2}$ and $^2\Pi_{1/2}$) of the OH product are in equilibrium. It suggests that BMHFP dissociates to produce OH from a PES, which does not interact with nearby triplet states, since the singlet–triplet interaction can contribute to a preference for the $^2\Pi_{3/2}$ state.

*4.1.4. Formation time of OH*

Time evolution of OH was measured by scanning the time delay between the photolysis and the probe lasers to understand how fast

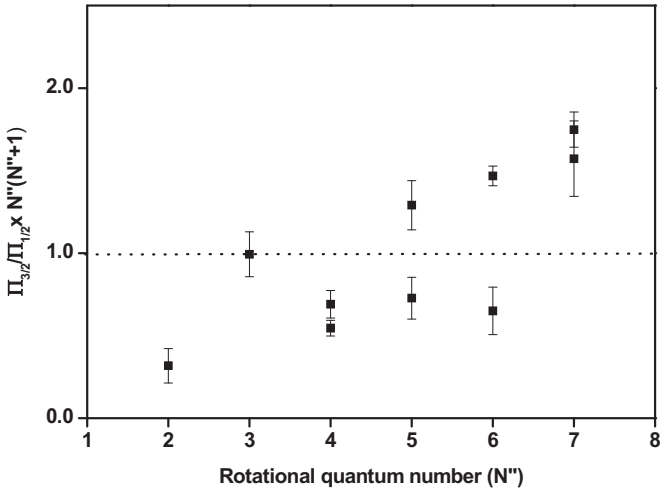


**Fig. 5.** A plot of the spin-orbit state population distribution ratio against rotational quantum number $N''$ for the OH radical produced in photodissociation of BMHFP with 193 nm laser. Both the spin-orbit populations are statistically produced.

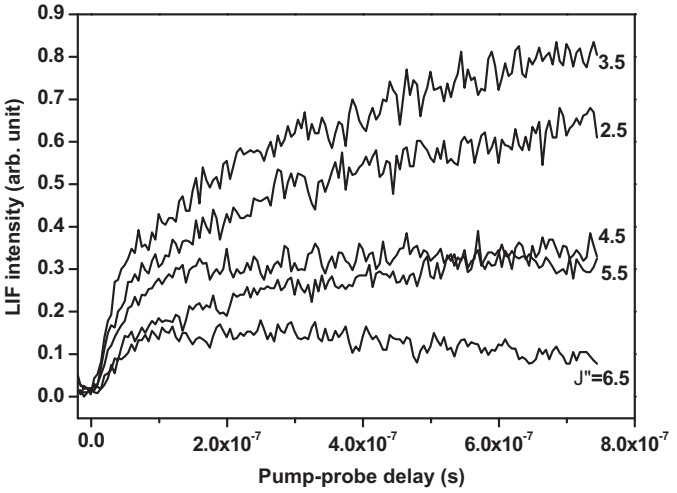


**Fig. 6.** Formation of OH in different rotational levels ($J''$). The plot shows the LIF signal for $J''$ = 2.5, 3.5, 4.5, 5.5 and 6.5 with pump-probe time delay.

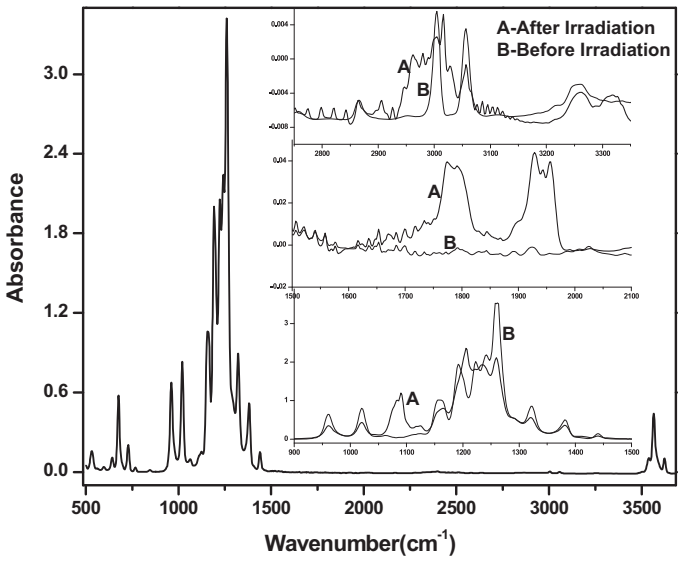


**Fig. 7.** IR spectrum of BMHFP (5 Torr) in the vapor phase using Zn–Se windows for the photolysis cell. In the inset, curve 'B' is before irradiation and 'A' is after irradiation with 500 pulses of 40 mJ cm$^{-2}$ of 193 nm laser.

or slow this product is produced on excitation of BMHFP at 193 nm. The formation kinetics of OH ($v''$ = 0, $J''$) was found to be strongly $J''$ dependent. A plot of LIF intensity against pump-probe time delay, for OH at different $J''$, is presented in Fig. 6. The time delay scans show that OH formation becomes faster with increasing $J''$ from 2.5 to 6.5. This $J''$ dependence of formation of the OH radical in a particular level is explained based on rotational relaxation of OH formed in higher levels. In lower rotational levels, i.e., $J''$ = 2.5 or 3.5, apart from the population formed initially, there is an increasing contribution from the relaxation of the higher rotational levels. Thus, the relaxation of OH from higher rotational levels to lower levels will delay its actual formation directly from BMHFP. Thus, the OH ($v''$ = 0, $J''$ = 2.5) shows much slower formation as compared to OH ($v''$ = 0, $J''$ = 5.5 or 6.5). Temporal evolution of OH ($v''$ = 0, $J''$ = 6.5), with highest measured value of $J''$, leads to the correct value of formation rate of OH, and the value obtained from this line is $8.9 \times 10^6$ s$^{-1}$. We observed similar $J''$ dependence of formation of the OH radical in photodissociation of BTFP [2] and butadiene monoxide [16] at 193 nm.

### 4.2. REMPI detection of Br on photodissociation of BMHFP at 234 nm

Photodissociation of BMHFP at ~234 nm generates Br, which was detected with (2 + 1) REMPI scheme as discussed earlier. Br is produced mostly in the ground spin orbit state ($^2P_{3/2}$) with the relative quantum yield of 0.64. A strong dependence of time of flight (TOF) profiles of Br and Br* on different laser polarizations suggests that the C–Br bond dissociation is very fast, and hence it is a primary process. The analysis of the profiles reveals 15.4 and 15.1 kcal mol$^{-1}$ of the relative translational energy in the Br and Br* channels, respectively. It implies the $\langle f_T \rangle$ value of 0.28 (with the available energy of 55.0 kcal mol$^{-1}$ at 234 nm) for the Br channel. We could not measure the translational energy release in the Br channel at 193 nm dissociation, due to some experimental constraints. Assuming the same $\langle f_T \rangle$ value at 193 nm dissociation, the average total translational energy released is 22.6 (0.28 × 80.9) kcal mol$^{-1}$.

### 4.3. Stable product analysis by FT-IR absorption

We measured the IR absorption spectrum of BMHFP in the vapor phase, to the best of our knowledge the same is not available in the literature and hence, we report the same in Fig. 7. The major peaks observed in the spectrum are at 3624, 3565, 3538, 3056, 3003, 1440, 1381, 1323, 1260 (strong), 1242, 1223, 1193, 1160, 1021, 962, 729 and 677 cm$^{-1}$. On photodissociation of BMHFP, at 193 nm, in addition to the transient product OH, we also detected some stable products employing FT-IR absorption spectroscopy. New IR features (inset of Fig. 7) in the irradiated mixture can be seen mainly between 1440 and 950 cm$^{-1}$ (at 1235, 1206, 1124 and 1090 cm$^{-1}$), between 2000 and 1600 cm$^{-1}$ (at 1956, 1944, 1928, 1793, 1775, 1670 and 1653 cm$^{-1}$), and at 3027, 3016, 2980, 2860, and 770 cm$^{-1}$. Some of these IR peaks are due to photoproducts, such as 1,1,1-trifluoroacetone ($F_3CC(=O)CH_3$), bromotrifluoromethane ($CF_3Br$) and (2-trifluoromethyl)-3,3,3-trifluoropropene ($F_3C–C(=CH_2)–CF_3$). The observed IR peaks, along with an assignment of some of these, are given in Table 1. 1,1,1-Trifluoroacetone and bromotrifluoromethane ($CF_3Br$) were characterized using their reported IR absorption spectra [17]. Some of the observed peaks have been tentatively assigned to $F_3C–C(=CH_2)–CF_3$, based on general features of a C=C bond. The observed uncharacterized peaks at 1956, 1944, 1928 cm$^{-1}$ also appeared in the irradiated BTFP [2] at 193 nm. The product analysis of BMHFP, and not BP, has been performed, since OH was detected only in the former.

### 4.4. Absorption cross-section and quantum yield measurements

The absorption cross-sections of BMHFP, BTFP and BP at 193 nm were measured to be $(3.6 \pm 0.3) \times 10^{-19}$, $(5.5 \pm 0.2) \times 10^{-19}$ and $6.6 \times 10^{-19}$ cm$^2$ molecule$^{-1}$, respectively. These values were used for the determination of the quantum yield of OH formation channel from BMHFP and BTFP on excitation at 193 nm. We calculated

**Table 1**
FT-IR absorption peaks, along with assignment of some of these, of product mixture on photolysis of BMHFP at 193 nm.

| Peak position, cm$^{-1}$ | Assignment of species | Reference |
|---|---|---|
| 1775 (strong), 1124 | $F_3CC(=O)CH_3$ | [17] |
| 1206, 1124, 1090 | $CF_3Br$ | [17] |
| 3027, 3016, 2980, 1670, 1653 | $F_3C–C(=CH_2)–CF_3$[a] | – |
| 2860, 1956, 1944, 1928, 1793, 1235, 770 | Unassigned | – |

[a] Spectra not reported, tentative assignment based on expected C=C and =C–H stretching frequencies.

**Table 2**
Absorption cross-section ($\sigma$), quantum yield of OH, $\Phi$(OH), and detection of Br product at 193 nm.

| Compound | $\sigma_{193}$ (cm$^2$ molecule$^{-1}$) | Br[a] (detected) | $\Phi_{193}$(OH) | Reference |
|---|---|---|---|---|
| BMHFP | $(3.6 \pm 0.3) \times 10^{-19}$ | Yes | 0.17 | This work |
| BP | $(6.6 \pm 0.3) \times 10^{-19}$ | – | 0.0[b] | This work |
| BTFP | $(5.5 \pm 0.2) \times 10^{-19}$ | Yes | 0.75 | This work |
| Acetic acid | $(1.1 \pm 0.2) \times 10^{-19}$ | No | 0.8 | [18] |

[a] Br not checked in BP.
[b] Under expt. limit.

the quantum yield of OH generation from BMHFP and BTFP by a relative method, using the relation,

$$\Phi_S = \frac{I_S}{I_R} \times \frac{\sigma_R}{\sigma_S} \times \Phi_R,$$

where $\Phi_S$ and $\Phi_R$ are quantum yields of a sample and a reference, respectively. The symbols $I$ and $\sigma$ stand for the LIF intensity and the absorption cross-section at 193 nm, respectively. Acetic acid was taken as a reference compound with the measured values of the absorption cross-section and the quantum yield of OH generation channel to be $1.1 \times 10^{-19}$ cm$^2$ molecule$^{-1}$ and 0.8, respectively [18]. The measured values of the absorption cross-section and the quantum yield of OH at 193 nm are provided in Table 2. All the rotational lines of OH($v'' = 0$) produced from BMHFP, BTFP and acetic acid at 193 nm were measured in identical experimental conditions, and the area of each rotational line was evaluated. The sum of the areas of all the rotational lines of OH from BMHFP or BTFP and acetic acid were compared, to obtain the quantum yields of OH formation channel from BMHFP and BTFP to be about $0.17 \pm 0.05$ and $0.75 \pm 0.08$, respectively.

### 4.5. Theoretical calculations

Molecular orbital (MO) calculations were carried out to investigate the potential energy surface (PES) for the dissociation channels, of BMHFP accessible on laser excitation at 193 nm. All the structures of the stable molecules and the transient species, including the TS, have been optimized at the B3LYP/6-311+G(d,p) level of theory and the zero-point energies were calculated at the same level of theory. Vibrational frequencies for all the species were calculated at the equilibrium geometry using the same level of theory as the geometry optimization. The calculated frequencies were positive, except for transition states, indicating that the equilibrium structures were at a minimum on the potential energy surfaces. All transition state structures were characterized by only one imaginary frequency and one negative eigenvalue of the force constant matrix. Besides the B3LYP energy, the energies of the optimized structures were also calculated at the second-order Moller–Plesset (MP2) level of theory, using the same basis sets. For all the radical channels the projected MP2 (PMP2) energies, wherein spin contamination has been taken care of, were calculated, which were lower as compared to the MP2 energies. All the energies used under discussion are at MP2/6-311+G(d,p) level of theory.

#### 4.5.1. Ground electronic state

The ground electronic states including transition state structures involved in photodissociation of BMHFP were optimized and energy of each optimized molecular species was calculated. The energy levels are schematically represented in Fig. 8, with the energy of each species marked in kcal mol$^{-1}$.

The conformational stability of BMHFP was investigated by density functional theory at B3LYP/6-311+G(d,p) level and *ab initio* MP2/6-311+G(d,p) calculations. The possible conformers of the molecule are determined by the rotation of the bromomethyl (BrCCO dihedral angle, $\phi_1$) and hydroxyl (HOCC(Br) dihedral angle, $\phi_2$) group. The calculated potential energy curves of the molecules with optimized geometry at B3LYP level and MP2 energies are consistent, with three distinct minima that correspond to gauche–syn, gauche–anti and anti–anti, structures are shown in Fig. 9. In the gauche–syn, gauche–anti and anti–anti conformers $\phi_1$ ($\phi_2$) values are $-48.5^\circ$ ($44.6^\circ$), $-58.0^\circ$ ($-175.5^\circ$) and $180^\circ$ ($180^\circ$), respectively. Among these three forms, the gauche–syn is calculated to be more stable by about 1.6 (1.3) and 0.9 (0.3) kcal mol$^{-1}$ than gauche–anti and anti–anti, respectively at B3LYP (MP2) level. The higher stability of the gauche–syn conformer can be attributed to an intramolecular hydrogen bond, and its evidence comes from the calculated structures. The Br···HO distance in the gauche–syn form is 2.58 Å, which is about 0.57 Å shorter than the sum of the van der Waals radii of bromine and hydrogen (3.15 Å) [19]. But, the Br···HO distance in the gauche–anti form is much longer (~4.12 Å). Even the Br···OH distance (3.18 Å) in the gauche–syn form is shorter than the sum of the van der Waals radii of bromine and oxygen (3.35 Å) [19]. Intramolecular hydrogen bond [19,20] has also been observed in 2-bromoethanol and 2-chloroethanol, providing stability of about 2.0 kcal mol$^{-1}$ [20,21]. Similar attractive fluorine–hydrogen interaction has been observed in 2-fluoroethanol as well [21,22]. Thus, in BMHFP also, an attractive interaction is expected between hydrogen of OH and not only bromine, but also fluorine, since the hydroxyl group and fluorine atoms (like bromine atom) are located on the adjacent carbon atoms. However, the calculated F···H distance is 2.58 Å, 2.34 Å and 2.34 Å in the gauche–syn, gauche–anti and anti–anti forms of BMHFP, respectively, in comparison to the sum of the van der Waals radii of fluorine and hydrogen of 2.55 Å [22]. Although the calculated F···H distance is the same in both the anti–anti and gauche–anti conformers, the F···H interaction is greater in the former than the latter, since it has two

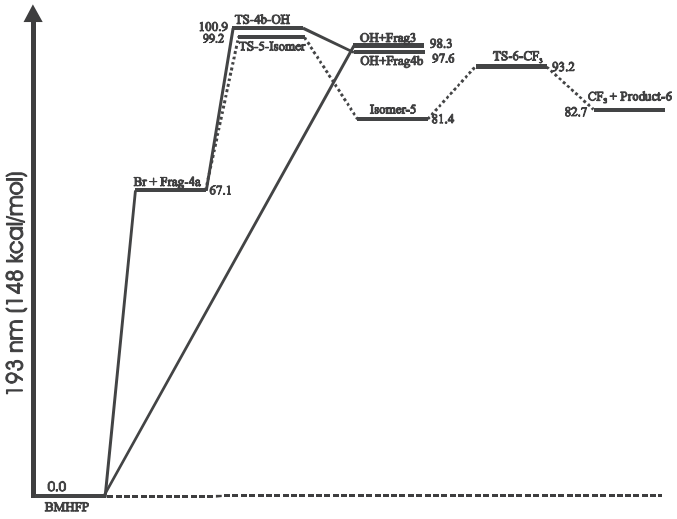


**Fig. 8.** Relative potential energy diagram for formation of OH (solid line) from the ground electronic state of BMHFP on excitation at 193 nm with two different possible pathways. This figure also depicts another possible dissociation channel (dotted line) from the primary dissociation product $F_3C$–$C(CH_2)$(OH)–$CF_3$ of BMHFP. The TS structures are marked according to the reaction numbers. Details are given in the text. All energies (in kcal mol$^{-1}$) are at MP2/6-311+G(d,p) level of theory.

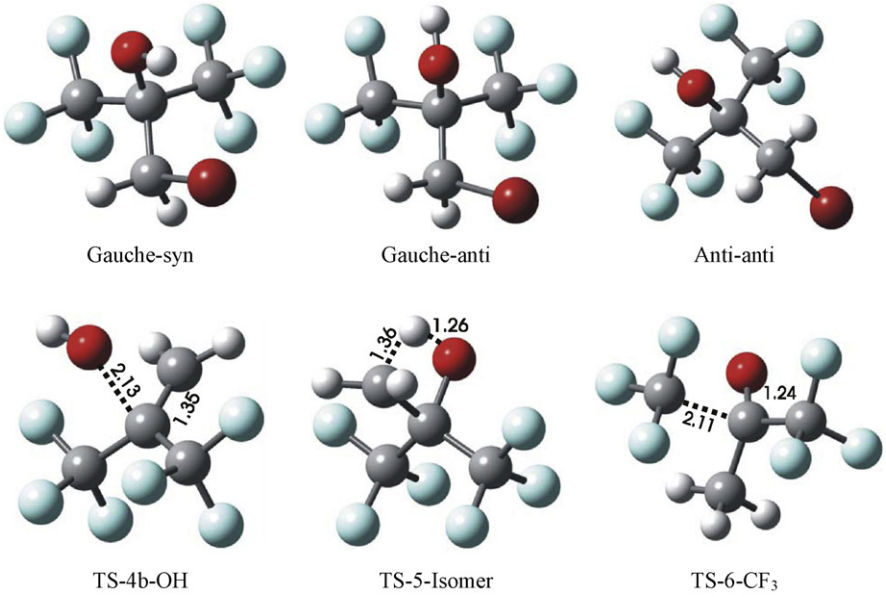


**Fig. 9.** The optimized structures of the ground electronic state of BMHFP (three conformers) and transition states of various reactions (marked according to the reaction number followed by reaction type). All structures are optimized at the B3LYP/6-311+G(d,p) level of theory.

similar intramolecular hydrogen bonds. Although the F···H interaction is not expected to be present in gauche–syn, this conformer of BMHFP is more stable than other two conformers, implying that the intramolecular Br···H interaction in the gauche–syn form is stronger than the F···H interaction in the anti–anti form. Similar results were observed in BTFP [2], where syn form is more stable than anti form.

#### 4.5.2. Excited electronic state

The photochemistry of BMHFP is not studied well. But, these are expected to be similar to BTFP, except for some differences arising from the presence of one more $CF_3$ group in lieu of H in BMHFP. However, the $CF_3$ group is not expected to produce any significant effect, since the nonbonding fluorine electrons are strongly bound. Excitation at 193 nm in BTFP [2] is assigned to $\sigma^*_{C-Br} \leftarrow n_{Br}$ transition. In BMHFP also, excitation at 193 nm is expected to lead to the same $\sigma^*_{C-Br} \leftarrow n_{Br}$ transition. The $\sigma^* \leftarrow n$ transition in alkyl halides (like in halogens and hydrogen halides) is complex because of a strong spin-orbit coupling of the unpaired electron remaining on the halogen atom [23,24]. This coupling is responsible for the spin-orbit splitting of the excited state, which leads to three allowed transitions known as $^1Q_1$, $^3Q_1$ and $^3Q_0$ transitions in the Mulliken notation [25]. Selective excitation of these transitions produces the halogen atom in either the ground or the excited spin-orbit state. Excitation of $^1Q_1$ and $^3Q_1$ transitions produces the ground state halogen atom, whereas that of $^3Q_0$ transition produces the spin-orbit excited halogen atom. Since both Br and Br* are produced from BMHFP on UV irradiation, the selective excitation of these transitions is not taking place.

We carried out population analysis to understand the nature of the excited states of BMHFP, and found that the excitation at 193 nm in BMHFP is similar to that in BTFP and bromoethanol [8], and it is assigned to the $\sigma^*_{C-Br} \leftarrow n_{Br}$ transition.

## 5. Discussion

### 5.1. Dissociation channels from BMHFP

The dissociation dynamics is well characterized by studying the dissociation channel experimentally in combination with theoretical calculations. In the photodissociation of BMHFP, the initial excitation at 193 nm involving $\sigma^*_{C-Br} \leftarrow n_{Br}$ transition leads to population of BMHFP in a higher electronic state, which is repulsive in nature. BMHFP is expected to undergo the C–Br bond cleavage impulsively from this repulsive state, producing Br and the radical $F_3C–C(CH_2)(OH)–CF_3$, the latter can dissociate to produce OH with the co-product $F_3C–C(=CH_2)–CF_3$. In stable product analysis, $F_3C–C(=O)–CH_3$ and $CF_3Br$ (on combination of $CF_3$ and Br radicals) are observed.

#### 5.1.1. OH formation

The formation of the OH radical from BMHFP on the excitation at 193 nm, can be ascribed to two different possible pathways, whose energetics are shown in Fig. 8. The OH radical can be produced as a primary product involving the C–OH bond cleavage (reaction (3)) with the bond dissociation energy of 98.3 kcal mol$^{-1}$.

$$F_3C–C(CH_2Br)(OH)–CF_3 \rightarrow F_3C–C(CH_2Br)–CF_3 + OH \quad (3)$$

OH can also be produced as a secondary product (reaction (4b)) from the primary product $F_3C–C(CH_2)(OH)–CF_3$ (reaction (4a)).

$$F_3C–C(CH_2Br)(OH)–CF_3 \rightarrow Br + F_3C–C(CH_2)(OH)–CF_3 \quad (4a)$$

$$F_3C–C(CH_2)(OH)–CF_3 \rightarrow F_3C–C(=CH_2)–CF_3 + OH \quad (4b)$$

The secondary pathway of OH formation is initiated by elimination of Br (reaction (4a)) with bond dissociation energy of 67.1 kcal mol$^{-1}$, in which the co-fragment subsequently dissociates via TS (structure is shown in Fig. 9 as TS-4b-OH) with an activation barrier ($E_b$) of 33.8 kcal mol$^{-1}$ to produce OH (reaction (4b)). One or both of these two mechanisms can be responsible for production of OH from BMHFP on excitation at 193 nm.

Theoretical studies suggest the lower excited electronic states of BMHFP are repulsive in nature with respect to the C–Br bond, and, therefore, the most facile primary event is expected to be the C–Br bond dissociation leading to Br formation (reaction (4a)). The REMPI measurements of Br and Br* on irradiation of BMHFP at 234 nm also suggest that the Br and Br* formation channels are primary processes taking place from a repulsive state. Since the calculated C–Br bond dissociation energy is 67.1 kcal mol$^{-1}$, formation of OH involving the C–OH bond in a primary reaction channel (reaction (3)) with a higher barrier of 98.3 kcal mol$^{-1}$ appears to

be less probable. Thus, the mechanism of OH formation on excitation of BMHFP at 193 nm involves first Br elimination, followed by the C–OH bond scission of the primary radical, to produce OH and $F_3C–C(=CH_2)–CF_3$ (reaction (4)). We could locate the corresponding TS structure (marked as TS-4b-OH in Fig. 9), in which the C–OH bond is elongated to 2.13 Å. The proposed mechanism of OH formation from BMHFP is similar to that from haloalcohols [8], 2-bromoethanol, wherein OH was proposed to be generated from a primary product $H_2C–CH_2OH$ (produced after Br elimination). In this haloalcohol the product OH and the co-fragment $C_2H_4$ are reported to have an isotropic centre-of-mass angular distribution, since the precursor $H_2C–CH_2OH$ is long-lived with respect to period of its rotation. Similar isotropic angular distribution of products, OH and its co-fragment, from BMHFP on excitation at 193 nm is expected, since the proposed mechanism of OH formation is similar and formation of OH was found to be relatively slow ($8.9 \times 10^6\ s^{-1}$). To verify this rate of formation of OH, we calculated the unimolecular rate of its formation to be $2.1 \times 10^6\ s^{-1}$ from the radical $F_3C–C(CH_2)(OH)–CF_3$ (a primary product) with the internal energy of 58.3 kcal mol$^{-1}$, which is estimated by subtracting the average translational energy release from the available energy in reaction (4a), employing RRKM (Rice–Ramsperger–Kassel–Marcus) unimolecular theory [26,27]. Thus, the RRKM rate does predict a low formation rate of OH, but it underestimates the experimental value of $8.9 \times 10^6\ s^{-1}$. This disagreement can originate possibly through a combined error from calculations of the C–Br bond dissociation energy in BMHFP and the internal energy of the radical in reaction (4a). This mechanism of OH formation is in good agreement with our earlier work on photodissociation of BTFP to produce OH.

#### 5.1.2. Other reaction channels

In a recent theoretical work on OH reaction with propene [28], possible dissociation channels have been predicted from an intermediate $H_3C–CH(OH)–CH_2$. In the present work, the intermediate radical $F_3C–C(CH_2)(OH)–CF_3$ in the proposed OH channel is similar to $H_3C–CH(OH)–CH_2$, with $H_3C$ and H each in the latter being replaced by $F_3C$. We have investigated possibility of similar low energy channels from $F_3C–C(CH_2)(OH)–CF_3$, to explain formation of an observed stable product $F_3C–C(=O)–CH_3$. In addition to the intermediate radical $F_3C–C(CH_2)(OH)–CF_3$ undergoing the C–OH bond scission (reaction (4b)), it can also isomerize to $F_3C–C(O)(CH_3)–CF_3$ (reaction (5)) through a TS (TS-5-isomer in Fig. 9), with $E_b$ of 32.1 kcal mol$^{-1}$. This isomer can undergo the C–$CF_3$ bond cleavage involving a TS, whose structure is shown in Fig. 9 as TS-6-$CF_3$, to produce the observed stable product $F_3C–C(=O)–CH_3$ (reaction (6), $E_b$ = 11.8 kcal mol$^{-1}$).

$$F_3C–C(CH_2)(OH)–CF_3 \rightarrow F_3C–C(O)(CH_3)–CF_3 \quad (5)$$

$$F_3C–C(O)(CH_3)–CF_3 \rightarrow F_3C–C(=O)–CH_3 + CF_3 \quad (6)$$

The energetics of these reactions are given in Fig. 8.

Another stable product, $CF_3Br$ is observed in the FTIR spectrum after irradiation with 193 nm. It means the $CF_3$ radical can react with Br to produce $CF_3Br$ as a stable product (reaction (7)).

$$CF_3 + Br + M \rightarrow CF_3Br + M \quad (7)$$

### 5.2. Partitioning of the available energy

The dissociation dynamics can be understood by examining the energy partitioning, which can be predicted by experimental results, theoretical calculations, and applying some dissociation models. The energy available ($E_{avl}$) to the primary products of the reaction (4a) is calculated from the photon energy ($h\nu$) at 193 nm, internal energy ($E_{int}$) of the parent molecule, and endothermicity ($\Delta E$) of the reaction (4a), using Eq. (8)

$$E_{avl}(4a) = h\nu + E_{int} - \Delta E(4a). \quad (8)$$

The energy change involved in the reaction generating Br (produced mostly in the ground spin-orbit state) and radical $F_3C–C(CH_2)(OH)–CF_3$, $\Delta E(4a)$, is estimated to be 67.1 kcal mol$^{-1}$. At 193 nm photodissociation, energy of photon, $h\nu$, being 148 kcal mol$^{-1}$, and after ignoring the small internal energy of the parent molecule at the room temperature, $E_{avl}(4a) = 148 - 67.1 = 80.9$ kcal mol$^{-1}$.

In a similar way, the energy available to the secondary products, reaction (4b), can be calculated using the relation,

$$E_{avl}(4b) = E_{avl}(4a) - \Delta E(4b) - E_T(4a), \quad (9)$$

where $\Delta E(4b)$ and $E_T(4a)$ are the endothermicity of reaction (4b), 30.5 kcal mol$^{-1}$, and the average amount of translation energy release (22.6 kcal mol$^{-1}$) in reaction (4a), respectively. Since the primary dissociation process occurs on a repulsive surface of BMHFP on excitation at 193 nm, the energy partitioning may be estimated employing the impulsive mechanism. The total translational energy released in reaction (4a) is evaluated to be 15.2 kcal mol$^{-1}$ (18% of the available energy), using the soft impulsive model [29] of energy partitioning. Thus, the impulsive model underestimates the translational energy release for the C–Br dissociation channel. This implies, $E_{avl}(4b)$ is 27.8 (80.9 − 30.5 − 22.6) kcal mol$^{-1}$. This available energy is partitioned into translational, rotational, and vibrational degrees of freedom of the photofragments OH and co-product $F_3C–C(=CH_2)–CF_3$ as specified by following expression,

$$E_{avl}(4b) = E_T(\text{OH + co-product}) + E_{int}(\text{OH}) + E_{int}(\text{co-product}) \quad (10)$$

OH is produced as a secondary product in the reaction (4b) from the primary product $F_3C–C(CH_2)(OH)–CF_3$. The OH translational energy $E_T$(OH) is measured to be 14.6 kcal mol$^{-1}$. We have estimated the total translational energy release, $E_T$(Total), in this case of two-step three-body dissociation of BMHFP, following similar methodology as Guest and co-workers [30] for the acetic acid dissociation, by using the equation:

$$E_T(\text{Total}) = E_T(\text{OH})\left[1 + \frac{m_{OH}}{m_{\text{co-product}}}\right] + E_T(\text{Rad})\left[\frac{m_{\text{co-product}}}{m_{Rad}} + \frac{m_{Rad}}{m_{Br}} - \frac{m_{OH}^2}{m_{\text{co-product}} m_{Rad}}\right] \quad (11)$$

where $m_{OH}$, $m_{\text{co-product}}$, $m_{Rad}$, and $m_{Br}$ are the masses of OH, its co-product $CF_3–C(=CH_2)–CF_3$, the radical $F_3C–C(CH_2)(OH)–CF_3$, and Br, respectively. $E_T$(Rad) is the translational energy of the precursor radical to OH. The translational energy released in Br, $E_T$(Br), is estimated to be 15.4 kcal mol$^{-1}$ employing REMPI. With $E_T$(Rad) and $E_T$(OH) of 7.2 (calculated using the measured value of $E_T$(Br)) and 14.6 kcal mol$^{-1}$ respectively, $E_T$(Total) is evaluated to be 38.8 kcal mol$^{-1}$, using Eq. (11). The total translational energy release, $E_T$(Total) in this case of two-step three-body dissociation is given as,

$$E_T(\text{Total}) = E_T(\text{Br}) + E_T(\text{OH}) + E_T(\text{co-product}) \quad (12)$$

Hence, $E_T$(co – product) is evaluated from the above expression to be 8.8 kcal mol$^{-1}$.

OH is produced mostly vibrationally cold with an average rotational energy of 0.93 kcal mol$^{-1}$ on photo-excitation of BMHFP at 193 nm. However, an average of 23.4 (14.6 + 8.8) kcal mol$^{-1}$ of the available energy (27.8 kcal mol$^{-1}$) is released into translation of reaction (4b). This suggests that the remaining part of the available

energy, 3.5 (27.8 – 23.4 – 0.9) kcal mol$^{-1}$ is partitioned as the internal energy of $F_3C–C(=CH_2)–CF_3$, the co-product of OH, in reaction (4b).

Bond dissociation energies, used for evaluating the amount of the available energy, are calculated using MO calculations. Similarly, the translational energy release in the primary reaction is not measured experimentally at 193 nm; rather it is estimated from the measurements at 234 nm. Therefore, an experimental measurement of the translational energy release directly at 193 nm in the primary dissociation channel combined with a high level of theoretical calculations for energies are required to improve the accuracy of an estimate of the available energy, which will result in improved evaluation of energies in the relative translation and the internal states of the products.

Since a significant fraction of the available energy is released in the relative translation of the products, either the OH channel (reaction (4b)) occurs impulsively from a repulsive state of $F_3C–C(CH_2)(OH)–CF_3$, or it has an exit barrier. The impulsive C–OH bond dissociation should lead to fast formation of OH, within the photolysis laser pulse of 20 ns. But, we observed relatively slow formation of OH with a rate coefficient of $8.9 \times 10^6$ s$^{-1}$, which is also supported by the RRKM unimolecular rate theory. Thus, the second possibility of the presence of an exit barrier in the C–OH bond scission, producing OH, can be responsible for a high amount of energy in the relative translation. This mechanism is validated through our theoretical calculations, which show the presence of the expected exit barrier. However, the estimated exit barrier of 1.4 (3.3) kcal mol$^{-1}$ at B3LYP(PMP2)/6-311+G(d,p) level of theory is quite small to explain quantitatively a large amount of energy in the relative translation of the products. A higher level of theory with larger basis sets will produce more accurate value of the barrier. Hence, we do not attach much significance to the calculated quantitative value of the exit barrier. Thus, a significant fraction of the available energy in the two-step three-body dissociation process is released in translation, mainly from the recoil of the products in the primary channel, which occurs on a repulsive surface, with some contribution from the exit barrier of the secondary reaction. A higher value of exit barrier for the OH channel can be expected for the BMHFP dissociation from a triplet surface, which can be populated through intersystem crossing due to heavy Br atom effect. However, it seems intersystem crossing from an initially prepared repulsive surface in BMHFP does not compete with the rapid impulsive dissociation of the C–Br bond.

### 5.3. Photodissociation of BP

Unlike from BMHFP and BTFP, we could not detect OH from 3-bromo-1-propanol (BP) on photoexcitation at 193 nm, in spite of its higher absorption cross-section at 193 nm, which was measured to be $(6.6 \pm 0.3) \times 10^{-19}$ cm$^2$ molecule$^{-1}$ as listed in Table 2. Thus, it implies that the OH formation mechanism in BP, similar to one proposed for BMHFP and BTFP, is not possible energetically, or this OH pathway does not compete with some other low energy channels. If a similar mechanism of OH formation operates in BP (reactions (13a) and (13b)),

$$BrCH_2–CH_2–CH_2OH \rightarrow Br + CH_2–CH_2–CH_2OH \quad (13a)$$

$$CH_2–CH_2–CH_2OH \rightarrow c\text{-}(CH_2–CH_2–CH_2) + OH \quad (13b)$$

our calculations suggest that energies required (shown in Fig. 10) for Br elimination from BP (reaction (13a)) and the subsequent C–OH bond cleavage (reaction (13b)), with an activation barrier of 49.0 kcal mol$^{-1}$, from the primary radical are greater than that from BMHFP. Thus, it implies that the OH channel may not compete with other low energy channels in BP.

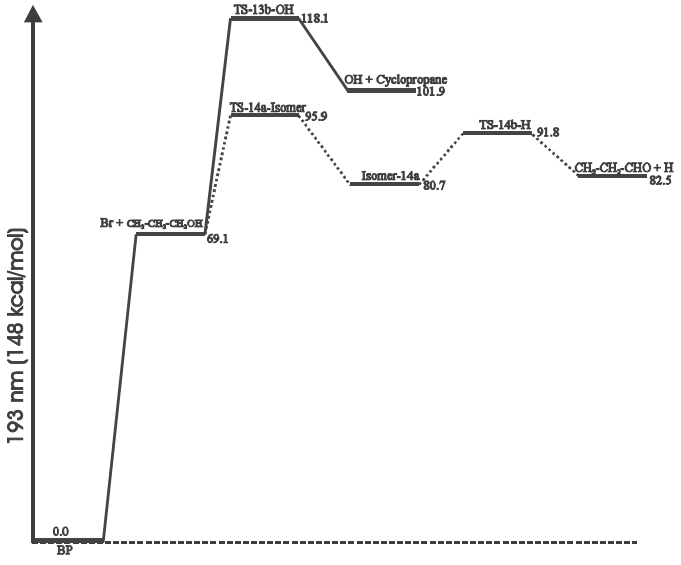


**Fig. 10.** Relative potential energy diagram for formation of OH (solid line) from the ground electronic state of BP. This figure also depicts another possible dissociation channel (dotted line) from the primary dissociation product of BP. The TS structures are marked according to the reaction numbers. Details are given in the text. All energies (in kcal mol$^{-1}$) are at MP2/6-311+G(d,p) level of theory.

Other low energy channels of BP are investigated theoretically. Energies involved in a re-arrangement of the radical formed on Br atom elimination (reaction (14a)), similar to reaction (5) of BMHFP, and subsequent dissociation (reaction (14b)) are calculated for BP, with results shown in Fig. 10.

$$CH_2–CH_2–CH_2OH \rightarrow CH_3–CH_2–CH_2O \quad (14a)$$

$$CH_3–CH_2–CH_2O \rightarrow CH_3–CH_2–CHO + H \quad (14b)$$

This sequence of reactions generating $CH_3–CH_2–CHO$ and H is energetically preferable with respect to that generating OH in BP. The energy level diagrams of Fig. 10 reveal that the activation barrier, $E_b$ of 49.0 kcal mol$^{-1}$ for the expected OH formation is greater than that of 26.8 kcal mol$^{-1}$ for the radical isomerization reaction (14a). But in BMHFP both $F_3C–C(=O)–CH_3 + CF_3$ and the OH channels are almost equally likely from the radical, formed after Br atom elimination in the primary step. The schematic energy level diagrams (Fig. 8) show that $E_b$ values for the radical isomerization (32.1 kcal mol$^{-1}$) and dissociation to produce OH (33.8 kcal mol$^{-1}$) are comparable in BMHFP. The isomerized radical subsequently leads to $F_3C–C(=O)–CH_3 + CF_3$ channel. Thus, OH could be detected from BMHFP, but not from BP, on excitation at 193 nm. Even another expected OH channel from BP, through propene + OH reaction, cannot compete with other low energy channels [28]. Thus, reaction energetics is responsible for OH formation in BMHFP, but not in BP.

### 5.4. Comparisons with saturated alcohols and saturated halo-alcohols

The small saturated alcohols [3–5] contribute to a common dissociation mechanism, after the $\sigma^*_{(O-H)} \leftarrow n_{(O)}$ excitation, involving the impulsive O–H bond breaking on the repulsive excited state PES along the O–H coordinate with large transitional energy release. The OH channel is either minor or not observed. Unlike these saturated alcohols, which do not contain halogen, BMHFP and BTFP (brominated saturated alcohols) produce OH on excitation at 193 nm. However, OH from these bromoalcohols is produced in a secondary reaction after elimination of bromine. The mechanism of OH formation from BMHFP and BTFP is similar to that from other saturated halo-alcohol, 2-bromoethanol. Thus, in these sat-

urated halo-alcohols, the nature of transition at 193 nm changes from $\sigma^*_{(O-H)} \leftarrow n_{(O)}$ in saturated alcohol to $\sigma^*_{(C-Br)} \leftarrow n_{(Br)}$, and OH is produced from the primary product. Since we could not detect OH from BP, in spite of its higher absorption cross-section of $6.6 \times 10^{-19}$ cm$^2$ molecule$^{-1}$ at 193 nm, it implies that all saturated halo-alcohols do not produce OH on excitation at 193 nm. One major structural difference between OH producing and non-OH producing saturated halo-alcohols is the relative position of halogen and OH moiety at α, β and α, γ, respectively. In the case of OH producing halo-alcohols, the radical formed on Br elimination, undergoes the C–OH bond cleavage to produce OH via a stable TS. The stability in the TS structure arises from double bond character, such stability to the corresponding TS is not feasible in non-OH producing halo-alcohols because of α, γ relative positions of Br and OH. Thus, the OH channel is not energetically competitive to other low energy channels.

Photodissociation dynamics of BMHFP at 193 nm appears to be similar as that of BTFP [2] and 2-bromoethanol [8]. OH is produced as a secondary product; following direct C–Br bond dissociation from a repulsive surface. The translational energy release in the primary step of BMHFP dissociation is measured to be 28% of the available energy. This value is measured to be 42% in 2-bromoethanol [8], and estimated to be about 22% in BTFP [2]. Although the overall mechanisms of OH formation are similar in both BMHFP and BTFP, the quantum yield of OH formation in the former is about four and half times lower than that in the latter.

## 6. Conclusions

The 193 nm photodissociation of saturated halogenated alcohols, 2-(bromomethyl)hexafluoro-2-propanol (BMHFP) and 3-bromo-1-propanol (BP), has been investigated employing laser-induced fluorescence technique to probe the nascent OH radical. Saturated bromoalcohols, such as 3-bromo-1,1,1-trifluoro-2-propanol (BTFP) and BMHFP, on excitation at 193 nm, generate OH in a secondary reaction. Along with the nascent OH radical, $CH_3COCF_3$ and $CF_3Br$ were observed as stable products in FTIR absorption study. Unlike BMHFP and BTFP, OH was not detected from 3-bromo-1-propanol (BP) under similar experimental conditions. With these studies it appears that all saturated bromopropanols, except for probably those having Br and OH on adjacent C atom, do not produce OH on excitation at 193 nm.

The dynamics of OH formation in BMHFP is nearly identical to that in BTFP. However, the quantum yield of OH formation is relatively lower (by a factor of 4) in BMHFP. Thus, the presence of an additional $CF_3$ group in BMHFP does not play any significant role in its photochemistry, except for the quantum yield, with respect to OH formation at 193 nm. OH ($v''$=0, $J''$) is produced as a secondary product from the primary product $F_3C–C(CH_2)(OH)–CF_3$, formed by direct C–Br bond dissociation from a repulsive surface. Measurements on the nascent state population distribution of OH reveal that it is produced mostly in the vibrational ground state ($v''=0$) with its rotational temperature of $465 \pm 25$ K. However, a significant fraction of the available energy in the two-step three-body dissociation process is released in the translational ($\langle f_T \rangle \sim 0.75$), mainly from the recoil of the products in the primary reaction channel, which occurs on a repulsive surface, with some contribution from the exit barrier of the secondary reaction. Our theoretical calculations predict this barrier to be 1.4 (3.3) kcal mol$^{-1}$ at B3LYP(MP2)/6-311+G(d,p) level of theory. A higher level of theory with larger basis sets can predict an accurate value of the exit barrier.

## Acknowledgements

We thank Dr P.N. Bajaj, Dr S.K. Sarkar and Dr T. Mukherjee for their constant support and encouragement.

## References

[1] L. Knutsen, E. Morrey, J. Riches, Halon Options Technical Conference (24–26 April 2001), p. 235.
[2] Y.N. Indulkar, H.P. Upadhyaya, A. Kumar, S.B. Waghmode, P.D. Naik, J. Phys. Chem. A 113 (2009) 8462.
[3] S. Harich, J.J. Lin, Y.T. Lee, X. Yang, J. Phys. Chem. A 103 (1999) 10324.
[4] K. Xu, G. Amaral, J. Zhang, J. Chem. Phys. 111 (1999) 6271.
[5] W. Zhou, Y. Yuan, J. Zhang, J. Chem. Phys. 119 (2003) 7179.
[6] S. Dhanya, A. Kumar, H.P. Upadhyaya, P.D. Naik, R.D. Saini, J. Phys. Chem. A 108 (2004) 7646.
[7] T.Y. Kang, S.K. Shin, H.L. Kim, J. Phys. Chem. A 107 (2003) 10888.
[8] E.J. Hintsa, X. Zhao, Y.T. Lee, J. Chem. Phys. 92 (1990) 2280.
[9] P.D. Naik, H.P. Upadhyaya, A. Kumar, A.V. Sapre, J.P. Mittal, J. Photochem. Photobiol.: Photochem. Rev. 3 (2003) 165.
[10] H.P. Upadhyaya, A. Saha, A. Kumar, T. Bandyopadhyay, P.D. Naik, P.N. Bajaj, J. Phys. Chem. A 114 (2010) 5271.
[11] M.J. Frisch, G.W. Trucks, H.B. Schlegel, G.E. Scuseria, M.A. Robb, J.R. Cheeseman, J.A. Montgomery Jr., T. Vreven, K.N. Kudin, J.C. Burant, J.M. Millam, S.S. Iyengar, J. Tomasi, V. Barone, B. Mennucci, M. Cossi, G. Scalmani, N. Rega, G.A. Petersson, H. Nakatsuji, M. Hada, M. Ehara, K. Toyota, R. Fukuda, J. Hasegawa, M. Ishida, T. Nakajima, Y. Honda, O. Kitao, H. Nakai, M. Klene, X. Li, J.E. Knox, H.P. Hratchian, J.B. Cross, C. Adamo, J. Jaramillo, R. Gomperts, R.E. Stratmann, O. Yazyev, A.J. Austin, R. Cammi, C. Pomelli, J.W. Ochterski, P.Y. Ayala, K. Morokuma, G.A. Voth, P. Salvador, J.J. Dannenberg, V.G. Zakrzewski, S. Dapprich, A.D. Daniels, M.C. Strain, O. Farkas, D.K. Malick, A.D. Rabuck, K. Raghavachari, J.B. Foresman, J.V. Ortiz, Q. Cui, A.G. Baboul, S. Clifford, J. Cioslowski, B.B. Stefanov, G. Liu, A. Liashenko, P. Piskorz, I. Komaromi, R.L. Martin, D.J. Fox, T. Keith, M.A. Al-Laham, C.Y. Peng, A. Nanayakkara, M. Challacombe, P.M.W. Gill, B. Johnson, W. Chen, M.W. Wong, C. Gonzalez, J.A. Pople, Gaussian 03, Gaussian Inc., Wallingford, CT, 2004.
[12] G.H. Dieke, H.M. Crosswhite, J. Quant. Spectrosc. Radiat. Transfer 2 (1961) 97.
[13] I.L. Chidsey, D.R. Crossley, J. Quant. Spectrosc. Radiat. Transfer 23 (1980) 187.
[14] W. Demtroder, Laser Spectroscopy, Springer, New Delhi, 2004.
[15] G. Herzberg, Molecular Spectra and Molecular Structure. I. Spectra of Diatomic Molecules, D. Van Nostrand Company, Inc., Princeton, New Jersey, 1957.
[16] S. Sengupta, Y. Indulkar, A. Kumar, P.D. Naik, P.N. Bajaj, J. Chem. Phys. 128 (2008) 024309.
[17] C.J. Pouchert, The Aldrich Library of FT-IR Spectra, Aldrich Chemical Co., Inc., Milwaukee, WI, 1989.
[18] P.D. Naik, A. Kumar, H.P. Upadhyaya, P.N. Bajaj, S.K. Sarkar, Laser Induced Fluorescence Spectroscopy, Wiley-VCH Publications, 2008.
[19] R.G. Azrak, E.B. Wilson, J. Chem. Phys. 52 (1970) 5299.
[20] P. Buckley, P.A. Giguere, M. Schneider, Can. J. Chem. 47 (1969) 901.
[21] K.B. Wilberg, M.A. Murcko, J. Mol. Struct. (THEOCHEM) 163 (1988) 1.
[22] K.S. Buckton, R.G. Azrak, J. Chem. Phys. 52 (1970) 5652.
[23] D. Krajnovich, L.J. Butler, Y.T. Lee, J. Chem. Phys. 81 (1984) 3031.
[24] W.H. Pence, S.L. Baughcum, S.R. Leone, J. Phys. Chem. 85 (1981) 3844.
[25] R.S. Mulliken, J. Chem. Phys. 8 (1940) 382.
[26] R.G. Gilbert, S.C. Smith, Theory of Unimolecular and Recombination Reactions, Blackwell Scientific Publications, Oxford and Cambridge, 1990.
[27] R.G. Gilbert, S.C. Smith, M.J.T. Jordan, UNIMOL Program Suite, 1993.
[28] L.K. Huynh, H.R. Zhang, S. Zhang, E. Eddings, A. Sarofim, M.E. Law, P.R. Westmoreland, T.N. Truong, J. Phys. Chem. A 113 (2009) 3177.
[29] A.F. Tuck, J. Chem. Soc., Faraday Trans. 2 (73) (1977) 689.
[30] S.S. Hunnicutt, L.D. Waits, J.A. Guest, J. Phys. Chem. 95 (1991) 562.